

Swift heavy ion irradiation of SrTiO₃ under grazing incidence

Ender Akcöltekin¹, Sevilay Akcöltekin¹, Orkhan Osmani¹,
Henning Lebius², Marika Schleberger¹‡

¹ Experimentelle Physik, Universität Duisburg-Essen, 47048 Duisburg, Germany

² CIMAP, Blvd. Henri Becquerel, 14070 Caen Cedex 5, France

Abstract. The irradiation of SrTiO₃ single crystals with swift heavy ions leads to modifications of the surface. The details of the morphology of these modifications depends strongly on the angle of incidence and can be characterized by atomic force microscopy. At glancing angles, discontinuous chains of nanosized hillocks appear on the surface. The latent track radius can be determined from the variation of the length of the chains with the angle of incidence. This radius is material specific and allows the calculation of the electron-phonon-coupling constant for SrTiO₃. We show that a theoretical description of the nanodot creation is possible within a two-temperature model if the spatial electron density is taken into account. The appearance of discontinuous features can be explained easily within this model, but it turns out that the electronic excitation dissipates on a femtosecond time scale and thus too rapidly to feed sufficient energy into the phonon system in order to induce a thermal melting process. We demonstrate that this can be solved if the temperature dependent diffusion coefficient is introduced into the model.

PACS numbers: 34.50.Bw, 61.80.Az, 61.82.Ms, 81.16.Rf

‡ electronic address:marika.schleberger@uni-due.de

1. Introduction

The irradiation of solid matter with heavy ions of 100 MeV energy has long been known to create structural modifications ranging from defects and amorphization in the bulk up to the creation of hillocks on the surface [1, 2, 3, 4].

In this energy range the projectile is slowed down almost exclusively by electronic interactions. The standard model to describe the energy transport is based on a two-temperature model and includes solving the heat diffusion equation in a cylindrical symmetry. This approach requires many approximations as well as the fitting of the strength of the electron-phonon coupling. The model has been quite successful explaining e.g. track radii in various materials created by irradiation perpendicular with respect to the surface [5].

If the sample is irradiated under grazing incidence it has recently been shown that chains of nanodots are created by single ions [6, 7]. In an earlier experiment similar elongated tracks on a LiF surface covered with gold particles have been observed and were explained in terms of an elastic shock wave model [8]. These phenomena cannot be longer described by the conventional thermal spike model for several reasons. ? the electron density cannot be approximated by a free electron gas because the electronic structure plays a major role in the creation of the chains.

To explain these striking experimental findings and to overcome the limitations of the conventional approach a model was proposed where the creation of hillocks is directly coupled to the spatial electron density of the material [6]. Every time the projectile travels through a region with a high density the energy loss is sufficiently high to feed energy into the electronic system, which finally results in a nanodot on the surface. Since the electron density corresponds to the periodicity of the crystal the nanodots appear on the surface with a certain periodicity depending on the exact impact parameters.

The aim of this paper is to study the track creation in SrTiO₃ in more detail. We extend the model proposed by Akcöltekin et al. [6] in order to determine the electron-phonon coupling constant and to study the diffusion of energy within the electron and the phonon system.

2. Experimental procedures

The single crystal samples of SrTiO₃(100) and SrTiO₃(111)(Crystec, Berlin) have been irradiated without prior surface treatment at the ion beam facility IRRSUD of the GANIL, France. The irradiation was done using ²⁰⁷Pb²⁸⁺ and ¹³¹Xe²³⁺ ions with kinetic energies of 130 and 93 MeV, respectively. These energies correspond to stopping powers of 22 keV/nm and 19 keV/nm, respectively, as calculated with SRIM [9]. The angle of incidence with respect to the surface was varied between $\Theta = 90^\circ$ and $\Theta = 0.3^\circ$. Fluences were typically chosen to yield between 5 and 20 impacts per μm^2 . After irradiation the samples were analyzed by atomic force microscopy (AFM) either in the intermittent

contact mode under ambient conditions or in contact mode in UHV. All AFM images were processed with the Nanotec Electronica SL WSxM software, version 4.0 Develop 8.3. [10]. From the raw data (400×400 data points) only a plane was subtracted. The colour code was changed using the palette *flow.lut*. No change of contrast (1) or brightness (0) was used.

3. Experimental results

Since the samples undergo no surface treatment prior to irradiation we make sure that the virgin surface is sufficiently characterized to be able to identify modifications due to irradiation. In the left part of fig.1 a typical AFM image of an untreated SrTiO_3 surface is shown. The irregular step edges separating the terraces can be clearly seen. The average step height is about $(3 \pm 0.5) \text{ \AA}$, this is in reasonable agreement with the literature value of 3.905 \AA [11]. The surface roughness is $rms \leq 1 \text{ nm}$.

After irradiation at $\Theta = 90^\circ$ nanosized hillocks have appeared on the otherwise unchanged surface. The sample shown in the right part of fig.1 was exposed to a fluence of $1 \times 10^9 \text{ ions/cm}^2$. On average we find 11 hillocks on this surface, i.e. every ion impact produces one of these nanodots.

If we change the angle of incidence from $\Theta = 90^\circ$ down to angles of 10° , the shape of the hillocks remains unchanged. However, if the angle is decreased even further the morphology of the irradiation induced damage changes drastically. This can be seen from fig.2. This series of AFM images demonstrates that the hillocks at first elongate along the direction of the ion trajectory (indicated by arrows), then elongated structures with two or three separate maxima appear, and finally chains of totally disconnected hillocks are created. Again, the number of chains corresponds to the fluence, so that each ion creates one chain. These chains can have a total length of a few microns, contain dozens of nanodots and these nanodots seem to exhibit a certain periodicity. The dimensions of the nanodots within the chains are comparable to the dimensions determined from the $\Theta = 90^\circ$ experiment (see insets).

By comparing samples irradiated with xenon ions with those irradiated with lead ions (not shown here), no significant differences in the morphology could be detected.

4. Discussion

It is clearly apparent from fig.2 that the length of the track varies with the angle of incidence. In order to quantify this we determined the length distributions as a function of the angle of incidence by analyzing around 60 tracks for each angle. As an example we present the length distribution for $\Theta = 0.5^\circ$ and $\Theta = 5^\circ$, respectively (see fig.3). Both are Gauss-shaped, for the extremely glancing angle it is centered around 750 nm whereas the mean length at 5° is 100 nm. The distribution for the glancing angles is much broader, most likely due to surface properties and the exact impact point (see also below).

The geometric relation describing the angle dependence has already been established in [6] and is applied here as well (see fig.4):

$$l = d / \tan \Theta \quad (1)$$

with the chain length l , and d being the maximum depth from which the excitation may reach the surface. This simple model assumes that a part of the latent track in the volume can be detected at the surface as a chain of hillocks. The ion excites the electronic system along the track and the energy is later transferred to the lattice via electron-phonon coupling. In a region where the local energy density is high enough, defects can be created, melting and amorphization may occur. Therefore, the ions trajectory is surrounded by a modified region with a radius given by d .

How far this local excitation can spread (i.e. the value of d) depends entirely on the material properties, such as the electron-phonon-coupling constant, the heat capacity, the heat conductivity, and the melting temperature. In a metal e.g., it is well known that the energy dissipation within the electronic system is so fast that on a time scale necessary for the lattice to react (a few 10 ps) the local energy density is already too low to create any permanent damage. As d should not depend on the different experimental conditions but only on the material we plotted all the data (irradiations with Xe and Pb as well as along the [100] and the [110] direction) in a single graph. As one can see from fig.4 our data can be fitted quite well with one curve, yielding $d = 8$ nm.

Understanding the position of the individual hillocks within the chain is more complicated and cannot be explained by this simple relation. The reason is that the spatial details of the electronic structure play an important role here. SrTiO_3 is an insulator and most valence electrons are located close to the oxygen atoms, a few around the titanium and almost none at the strontium sites. The energy loss of the projectile is dominated by electronic stopping which can only occur in regions where the electron density is high enough. That is, the ion experiences a strongly varying force corresponding to the local variations of the electron density. We therefore follow the approach first described in [6] and use the DFT electron density [12] to calculate the stopping power dE/dx along the ion trajectory [13]. The result for an ion traveling almost (deviation $\approx 0,4^\circ$) along the [001] and the [110] direction is shown in fig.5, left part of top and lower panel, respectively.

We then calculate the moving average (averaging width 10 nm, red line in fig.5) of this data to take into account that hillocks can only be created if the average energy density in this region is high enough. The distance between the local maxima in the averaged stopping power is 55 nm and correspond well with the experimentally observed distances between hillocks. However, we wish to point out that in certain geometries a slight deviation from the azimuthal angle can have a rather large influence on the exact positions of the maxima in the stopping power along the trajectory. For example, a trajectory which deviates only 1° from the low indexed [011] direction towards the [112] direction (see fig.5) appears already very irregular. Therefore, the hillocks within the chains are usually not as equally spaced as one would probably expect. In addition,

the electron excitation is a statistical process, i.e. hillocks may appear differently even along identical trajectories.

To demonstrate the influence of the azimuthal angle more clearly we have irradiated a (100) oriented crystal surface along the [001] direction and a (111) surface along the [110] direction (exact within a few degrees). By using crystals of different orientations it is possible to probe higher indexed directions and still use glancing incidence angles. The result is shown in fig.6. The tracks appear very similar at first but a detailed analysis reveals minor differences: On the (111) surface the nanodots tend to appear in closely neighboring pairs (right panel of fig.6) whereas on the (100) surface the dots appear to be more regularly spaced (left panel of fig.6, compare with top right panel of fig.5). In fact, the chain in the right part of fig.6 exhibits a periodicity of (58 ± 8) nm, which corresponds to a lattice constant of 3.9 \AA if we assume that the ion hit the surface under $\Theta = 0.4^\circ$. This clearly indicates that the dots represent a direct projection of the electron density onto the surface. Such a quantitative comparison of any given trajectory with the calculations is however not possible because the experimental parameters, especially the angle of incidence, cannot be controlled with the required precision.

From the analysis above it is evident that the electronic excitation must be the source for the creation of nanodots. However, the creation of dots requires the movement of atoms, i.e. the transfer of energy from the electronic into the phononic system. Within the two-temperature model this is implemented by introducing a electron-phonon-coupling constant g which controls the energy flux. As source terms the space and time dependent energy loss along the trajectory enters the calculation. In addition, the spatial and temporal evolution of the energy density has to be calculated which is done by solving the heat diffusion equation.

Since the parameter d is material specific it can be used to determine the electron-phonon-coupling constant as follows: from fig.4 we can determine the track length that the ion has to travel before it can no longer create modifications on the surface. In the case of $\Theta = 0.3^\circ$ and $d = 8$ nm (see [6] and fig.4) this length would be ≈ 1530 nm. We calculate the energy loss at the end of that trajectory and project it onto the surface. We subsequently calculate the temperature at the surface for different values of g . For the conversion of energy into temperature we use the experimentally determined heat capacity of SrTiO₃ of $C = 100 \text{ J/(K mol)}$ [14]. If we assume that in order to modify the surface, at least the melting temperature of SrTiO₃ ($T_{melt} = 2353 \text{ K}$ [11]) has to be achieved, we find that $g \approx 1 \times 10^{18} \text{ W/(m}^3 \text{ K)}$ as can be seen from fig.7. Experimentally determined values of g for other materials are in good agreement with our finding [?, 15].

After g and the source terms $B(\vec{r}, t)$ for the electronic excitation have been determined the diffusion equations describing the energy relaxation within the two temperature model can be solved using finite differences and with von Neumann boundary conditions. As initial temperature zero K was chosen.

$$\frac{\partial E_e}{\partial t} = D_e(\nabla E_e) - g \cdot (E_e - E_l) + B(\vec{r}, t) \quad (2)$$

$$\frac{\partial E_l}{\partial t} = D_l(\nabla E_l) + g \cdot (E_e - E_l) \quad (3)$$

Analyzing the data we find that with reasonable parameters ($D_l = 0.0005 \text{ cm}^2/\text{s}$, $D_e = 0.05 \text{ cm}^2/\text{s}$) the energy in the electronic system dissipates on a time scale of a few ten femtoseconds (see fig.8), whereas the energy transfer into the phonon system requires picoseconds. That is, the energy density that remains after 30 fs is much too low to induce a temperature close to the melting temperature. To create a high enough energy density in this scenario g would have to be three orders of magnitude larger which is non-physical.

If the energy transfer happens via electron-electron and electron-phonon scattering the diffusion coefficient is directly related to the scattering cross section of two particles. In the case of highly excited electrons the scattering cross section between a hot electron and a cold one is small because they are energetically too different from each other. Only by transferring energy to the phononic system the energy (and the temperature) of the electrons decreases and thus the diffusivity increases. To take this into account we use a temperature dependent diffusion coefficient (see e.g. [16]) for the electronic system instead of a constant diffusion. This approach treats the excited electrons as an electron gas with a very low density [17] (for a detailed discussion see [18]):

$$D(T) = \frac{2k_B}{\pi m_e} \frac{T_e}{T_e^2 + T_l} \quad (4)$$

with k_B the Boltzmann constant, m_e the electron mass, $T_e = \sqrt{2E_e/C}$ and $T_l = 2E_l/(3Nk_b)$.

This approach ensures that the electronic dissipation is delayed. As D is proportional to $1/T$ for $T_l \ll T_e$ the diffusion is very ineffective at high lattice temperatures. Thus, the excitation is confined to a small region and lasts long enough to feed sufficient energy into the much slower phonon system characterized by a constant diffusion coefficient of $D_l = 0.0005 \text{ cm}^2/\text{s}$. Solving the diffusion equations within this approach, maxima of phonon energies are compatible with the melting temperature and typically occur on time scales of $\approx 50 \text{ ps}$ (see fig.9 and additional material), which is quite reasonable.

That is, within the two-temperature model the time-scale problem discussed above can be overcome by the introduction of a temperature dependent diffusion coefficient. This does however not solve the basic problem of the two-temperature model itself, that the system is not in thermal equilibrium during the excitation process and thus important physical quantities such as the temperature are ill-defined. The conversion of energy into electron temperatures e.g. by using the heat capacity would only be correct if we assume that the thermalization of the electronic excitation happens either very fast or the distribution is fermi-like from the beginning. For metals it has been shown that the thermalization of a non-thermally excited electron gas requires 10-100 fs [19, 20]. In the case of an insulator, this time should be even longer due to longlived excitations such as excitons. In this sense, the temperatures should be interpreted as a quantity to parameterize the energy density but not as a real temperature.

Finally, we would like to discuss the possibility that the creation of nanodots may not at all be the result of a thermal process but is linked to a direct coherent excitation of atoms. This so-called non-thermal melting has been observed for semiconductors like InSb and is due to the efficient excitation of optical phonons by intensive laser pulses [21]. A prerequisite for this process is the excitation of an electron-hole plasma by the intense laser pulse [22]. With ions, fields strength of similar intensity can be achieved and thus a dense enough electron-hole plasma could be created. On the basis of the current data it is not possible to check whether this process exists. In any case it could not be treated within the two-temperature model and is thus beyond the scope of this paper.

5. Conclusions

We have shown that with swift heavy ions chains of individual hillocks can be created on SrTiO_3 surfaces if the irradiation takes place under glancing angles. The length of the chains can be easily controlled by varying the glancing angle. While the length of the chains is independent of the azimuthal angle, the hillock separation within the chains is not. This is a clear indication that the exact spatial distribution of the electrons has to be taken into account in order to understand the hillock formation. We have demonstrated how within the two-temperature model the electron phonon coupling constant can be obtained from the dependence of the chain length on the angle of incidence.

Applying the two-temperature model to our data we find that the electronic excitation dissipates too fast to deliver enough energy to the phonon system. This problem can be overcome by using a temperature-dependent diffusion coefficient, yielding reasonable time scales for the phonon heating in the range of several 10 ps. However, one has to keep in mind that only relatively few electrons with rather high energies are created by the moving ion. Thus, a model based on temperatures and describing a diffusive transport might not be appropriate at all. Instead, the transport would be better described applying a Boltzmann transport formalism which is part of the ongoing research in our group.

Acknowledgement

We thank R. Meyer for calculating the electron density and for stimulating discussions. We thank A. Duvenbeck for many helpful discussions and his continuous support. Financial support by the DFG - SFB616: *Energy dissipation at surfaces* is gratefully acknowledged. The experiments were performed at the IRRSUD beamline of the Grand Accélérateur National d'Ions Lourds (GANIL), Caen, France.

References

- [1] K. Awazu, X. Wang, M. Fujimaki, T. Komatsubara, T. Ikeda, and Y. Ohki. Structure of latent tracks in rutile single crystal of titanium dioxide induced by swift heavy ions. *Journal of Applied*

- Physics*, 100:044308, 2006.
- [2] N. Khalfaoui, M. Görlich, C. Müller, M. Schleberger, and H. Lebius. Latent tracks in CaF₂ studied with atomic force microscopy in air and in vacuum. *Nucl. Instrum. Methods B*, 245:246–249, 2006.
 - [3] A.S.El-Said, M.Cranney, N.Ishikawa, A.Iwase, R.Neumann, K.Schwartz, M.Toulemonde, and C.Trautmann. Study of heavy-ion induced modifications in BaF₂ and LaF₃ single crystals. *Nucl. Instr. and Meth. B*, 218:492–497, 2004.
 - [4] A. Müller, R. Neumann, K. Schwartz, and C. Trautmann. Scanning force microscopy of heavy-ion tracks in lithium fluoride. *Nucl. Instr. and Meth. B*, 146:393–398, 1998.
 - [5] M. Toulemonde, C. Dufour, and E. Paumier. Transient thermal process after a high-energy heavy-ion irradiation of amorphous metals and semiconductors. *Phys. Rev. B*, 46:14362, 1992.
 - [6] Ender Akcöltekin, Thorsten Peters, Ralf Meyer, Andreas Duvenbeck, Miriam Klusmann, Isabelle Monnet, Henning Lebius, and Marika Schleberger. Creation of multiple nanodots by single ions. *Nature Nanotechnology*, 2:290–294, 2007.
 - [7] A. M. J. F. Carvalho, M. Marinoni, A. D. Touboul, C. Guasch, H. Lebius, M. Ramonda, J. Bonnet, and F. Saigné. Discontinuous ion tracks on silicon oxide on silicon surfaces after grazing angle heavy ion irradiation. *Appl. Phys. Lett.*, 90:073116, 2007.
 - [8] I.V.Vorobyova. Tracks formation on lif crystal surface due to grazing incidence of 1mev/u sn ions. *Nucl. Instr. and Meth. B*, 146:379–384, 1998.
 - [9] J.F. Ziegler and J.P. Biersack. The stopping and range of ions in matter (SRIM). <http://www.srim.org>, 2008.
 - [10] I. Horcas, R. Fernández, J. M. Gómez-Rodríguez, J.Colchero, J. Gómez-Herrero, and A. M. Baro. Wsxn: A software for scanning probe microscopy and a tool for nanotechnology. *Rev. Sci. Instr.*, 78:013705, 2007.
 - [11] Landolt-Börnstein. Handbook of material properties. Edition 2006.
 - [12] The DFT calculations were performed using the ABINIT package [?] together with pseudopotentials generated by the fhi98pp code [?]. For the exchange-correlation energy the Perdew-Burke-Enerzhof generalized-gradient approximation functional [?] was used. The electron density was derived at the equilibrium lattice constant ($7.53 a_{\text{Bohr}}$ for SrTiO₃). In all calculations a common kinetic-energy cutoff-energy of 96 Hartree for the expansion of the wave functions and a $8 \times 8 \times 8$ k-point mesh were used.
 - [13] O. Osmani, A. Duvenbeck, H. Lebius, and M. Schleberger. Ab-initio calculation of electronic stopping power along glancing swift heavy ion tracks in perovskites. *Submitted to J. Phys. C, arXiv:0801.3381v1 [cond-mat.mtrl-sci]*.
 - [14] D. de Lingy and P. Richet. High-temperature heat capacity and thermal expansion of SrTiO₃ and SrZrO₃ perovskites. *Phys. Rev. B*, 53:3013, 1996.
 - [15] M. Caron, H. Rothard, M. Toulemonde, B. Gervais, and M. Beuve. Theoretical and experimental study of electron temperatures in heavy ion tracks from Auger electron spectra and thermal spike calculations. *Nucl. Instr. Methods B*, 245:36, 2006.
 - [16] A. Duvenbeck and A. Wucher. Low-energy electronic excitation in atomic collision cascades: A nonlinear transport model. *Phys. Rev. B*, 72:165408, 2005.
 - [17] I.A. Baranov, Yu.V. Martynenko, S.O. Tsepelevich, and Yu.N. Yavlinskii. Inelastic sputtering of solids by ions. *Sov. Phys. Usp.*, 31:1015, 1988.
 - [18] O. Osmani, A. Duvenbeck, H. Lebius, and M. Schleberger. Diffusion of highly excited electrons in insulators. *To be published*.
 - [19] C.A. Schmuttenmaer, M. Aeschlimann, H.E. Elsayed-Ali, R.J.D. Miller, D.A. Mantell, J. Cao, and Y. Gao. Time-resolved two-photon photoemission from Cu(100): Energy dependence of electron relaxation. *Phys. Rev. B*, 50:8957, 1994.
 - [20] B. Rethfeld, A. Kaiser, M. Vicanek, and G. Simon. Ultrafast dynamics of nonequilibrium electrons in metals under femtosecond laser irradiation. *Phys. Rev. B*, 65:214303, 2002.
 - [21] A. Rousse, C. Rischel, S. Fourmaux, I. Uschmann, S. Sebban, G. Grillon, Ph. Balcou, E. Förster,

- J.P. Geindre, P. Audebert, J.C. Gauthier, and D. Hulin. Non-thermal melting in semiconductors measured at femtosecond resolution. *Nature*, 410:65, 2001.
- [22] P. Stampfli and K.H. Bennemann. Theory for the instability of the diamond structure of Si, Ge, and C induced by a dense electron-hole plasma. *Phys. Rev. B*, 42:7163, 1990.

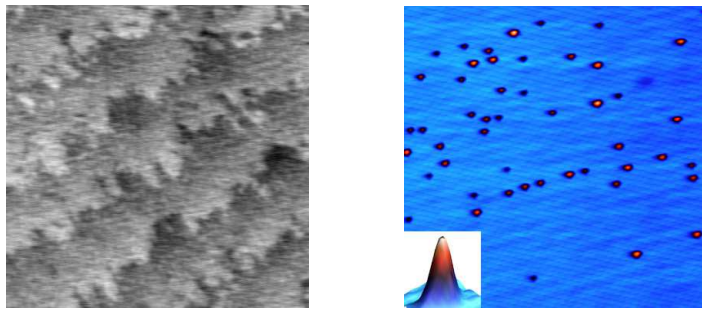


Figure 1. Left panel: AFM image of a clean $\text{SrTiO}_3(100)$ surface taken *in situ*, roughness is $rms < 1$ nm. Frame size is 800×800 nm². Right panel: Surface after irradiation with 130 MeV Pb ions, $\Theta = 90^\circ$, fluence 3×10^9 ions/cm². Inset shows a 3-dimensional image of a single hillock which has a height of 4.5 nm. Image size is 2×2 μm^2 .

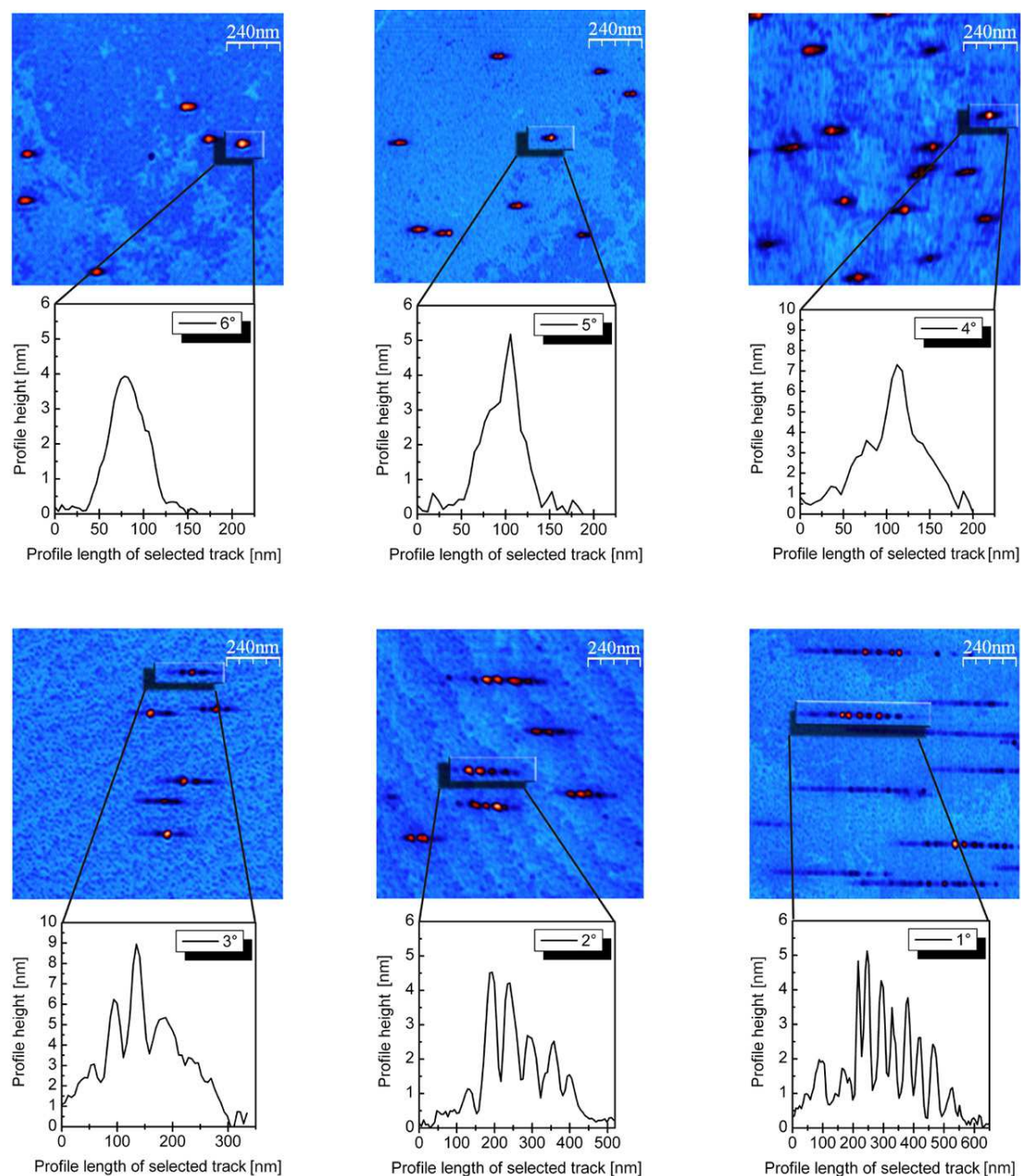


Figure 2. AFM images of SrTiO_3 surfaces irradiated with 93 MeV Xe ions. Upper row, from left to right: angle of incidence 6° , 5° , 4° . Lower row, from left to right: angle of incidence 3° , 2° , 1° . Image size is $1.2 \times 1.2 \mu\text{m}^2$, scale runs from 0 nm (blue) to 5 nm (orange). Line scans are taken from highlighted regions.

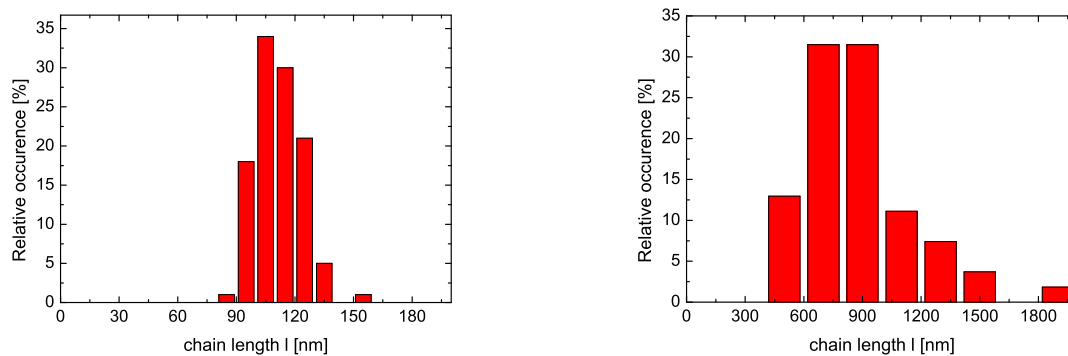


Figure 3. Length distribution for two different angles of incidence ($\Theta = 5^\circ$ and $\Theta = 0.5^\circ$) determined from 105 and 60 individual tracks, respectively.

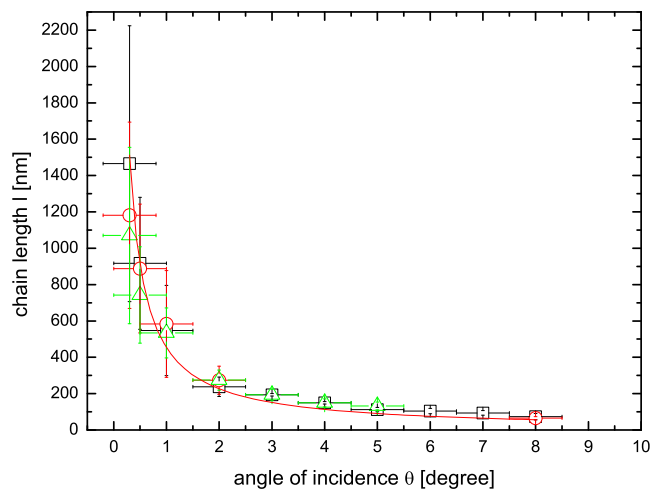


Figure 4. Length of chains as a function of angle of incidence. Data from various experiments. Circles: 96 MeV $\text{Xe}^{23+} \rightarrow \text{SrTiO}_3(111)$. Squares: 96 MeV $\text{Xe}^{23+} \rightarrow \text{SrTiO}_3(100)$. Triangles: 130 MeV $\text{Pb}^{28+} \rightarrow \text{SrTiO}_3(100)$. The line represents a fit according to eq. 1 with $d = 8$ nm.

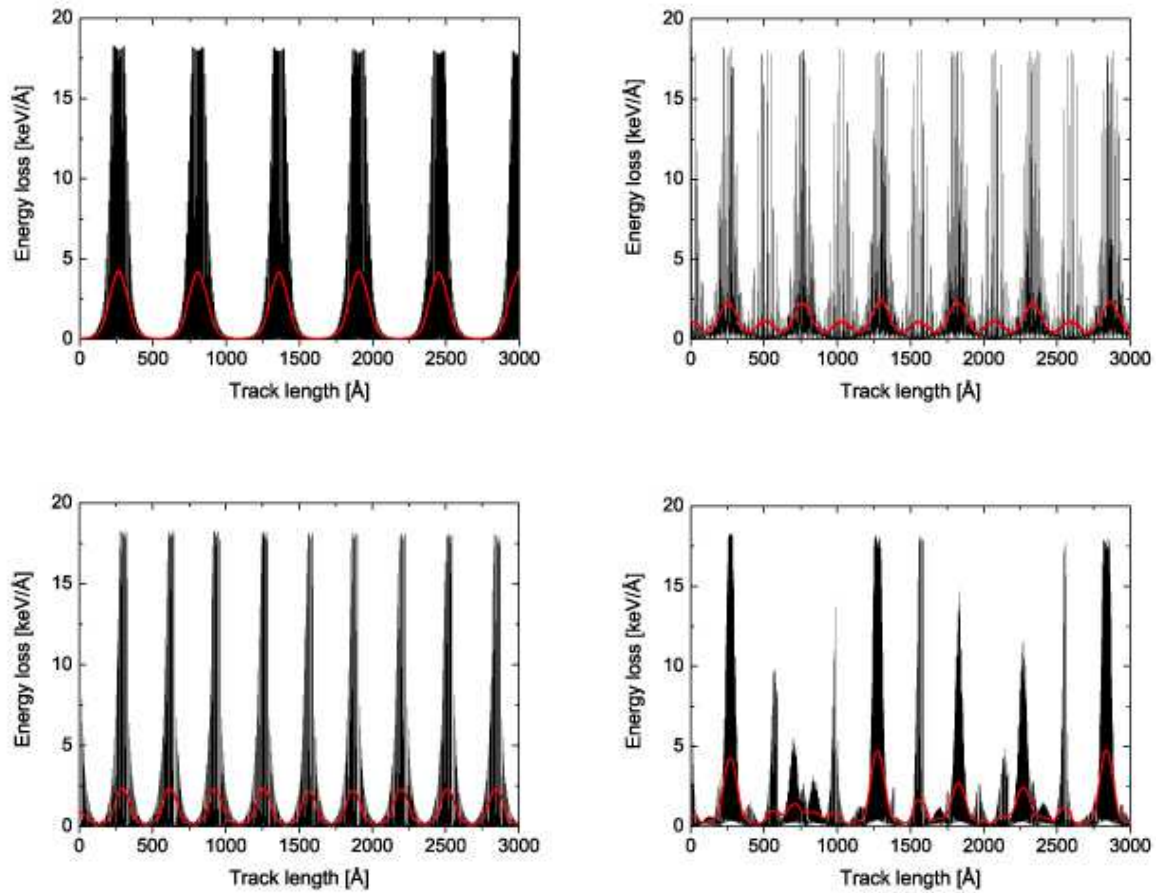


Figure 5. Calculated electronic stopping along different example trajectories with different θ and ϕ . Top left panel: $\Theta = 0.4^\circ$ with respect to the [001] direction and ϕ along the [001] direction; top right panel: $\Theta = 0.4^\circ$ and $\phi = 10^\circ$ with respect to the [001] direction. Lower left panel: $\Theta = 0.4^\circ$ with respect to the [011] direction and ϕ along the [011] direction; lower right panel: $\Theta = 0.4^\circ$ with respect to the [011] direction and $\phi = 1.0^\circ$ with respect to the [011] direction. The red line represents the moving average of the data, averaging width 10 nm.

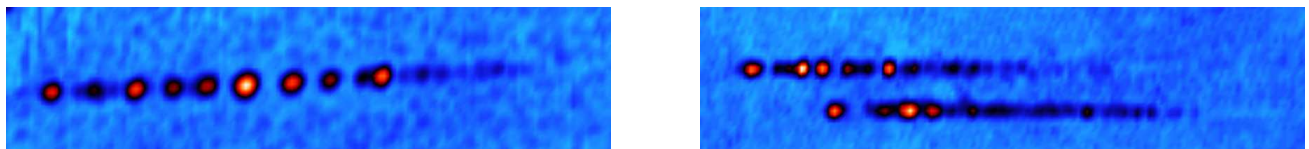


Figure 6. Left: AFM image of a track created on a $\text{SrTiO}_3(100)$ surface, $\theta = 0.5^\circ$, $\phi \approx$ along the [001] direction. Right: AFM image of a track created on a $\text{SrTiO}_3(111)$ surface, $\theta = 0.5^\circ$, $\phi \approx$ along the [110] direction. Image size is $200 \times 850 \text{ nm}^2$.

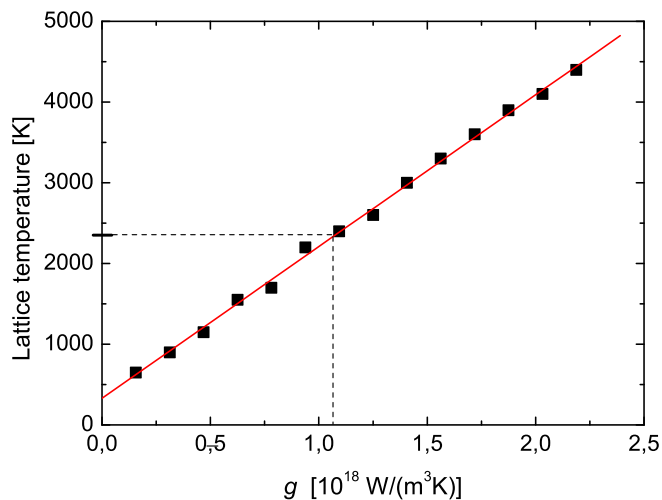


Figure 7. Temperature in K on the surface as a function of the electron-phonon coupling constant g . The bar on the temperature axis marks the melting temperature of SrTiO_3 . The red line represents a linear fit to the data.

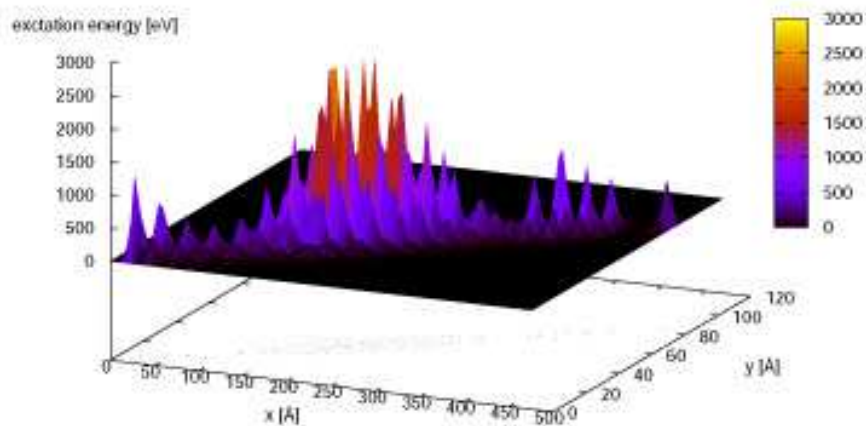


Figure 8. Energy density on the surface for $g \approx 1 \times 10^{18} \text{ W}/(\text{m}^3\text{K})$ after $t = 32 \text{ fs}$. The diffusion of the energy within the electronic system is treated with a constant diffusion coefficient (see text).

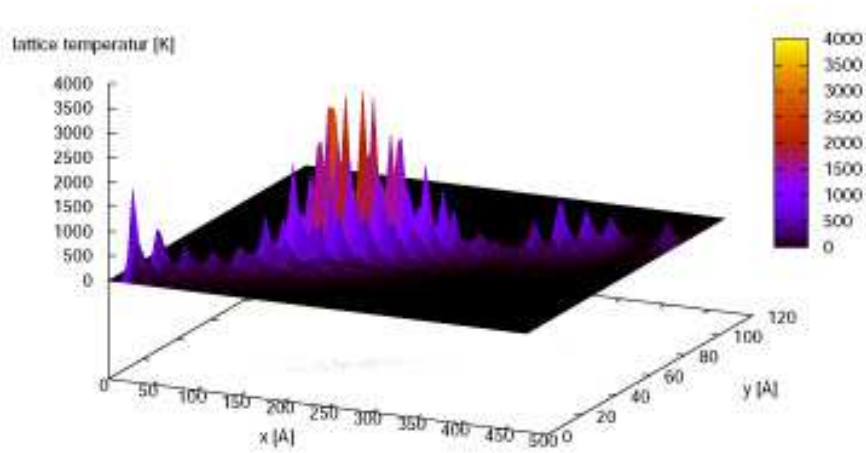


Figure 9. Temperature on the surface in K for $g \approx 1 \times 10^{18} \text{W}/(\text{m}^3\text{K})$ after $t = 34$ ps. The diffusion of the energy within the electronic system is treated with a temperature dependent diffusion coefficient (see text).